MATERIALS CHEMISTRY FRONTIERS

RESEARCH ARTICLE

View Article Online
View Journal | View Issue

Cite this: *Mater. Chem. Front.*, 2023, **7**, 3706

Glucose oxidase and conjugated polymer nanocomplexes for synergistic photothermal/starvation/oxidation therapy†

Wei Zhang,*[a] Wenhai Lin,[b] Zhensheng Li,[c] Tingting Sun*[d] and Zhigang Xie*[d]

Photothermal therapy (PTT) is becoming a prevalent tumor therapeutic method, but the overexpression of heat shock proteins (HSPs) and the self-repair mechanism of malignant tumors may restrict its therapeutic effect. Glucose oxidase (GOx) has been reported to effectively block the uptake of nutrients by tumor cells *via* starvation therapy, further debasing the production of HSPs in cells. Thus motivated, a nanoplatform (IBDDP&GOx NPs) integrating PTT, starvation therapy and oxidation therapy was constructed using a near-infrared BODIPY-based conjugated polymer (IBDDP) and GOx. Through the electrostatic interaction between the positively charged imidazole group from IBDDP and the negatively charged GOx, IBDDP and GOx could assemble into stable nanocomplexes, simultaneously solving the problem of insolubility of BODIPY-based conjugated polymers in aqueous solution as well as the poor stability and grievous system toxicity of GOx. Additionally, IBDDP&GOx NPs effectively retain the excellent photothermal properties of IBDDP and the biological catalytic activity of GOx, thus exhibiting enhanced inhibitory effects on tumor cell survival and malignant proliferation. This work proposed a simple example of integrating conjugated polymers with functional proteins into one formulation, which could overcome the shortcomings of single therapy and achieve a better synergistic treatment effect by multimodal cancer therapy.

Received 7th February 2023,
Accepted 28th April 2023

DOI: 10.1039/d3qm00132f

rsc.li/frontiers-materials

Introduction

Photothermal therapy (PTT) mainly takes advantage of nontoxic photothermal agents (PTAs) to generate local high temperature under laser irradiation to noninvasively inhibit the growth of malignant tumors.[1–3] However, it has been reported that tumor cells could generate heat shock proteins (HSPs) under hyperthermic stress to defend against heat-induced cellular damage, especially HSP70/90, which would enhance hyperthermic tolerance and treatment resistance.[4–6] Consequently, the dose of PTAs and the laser power density should be adjusted to a higher level to enhance photothermal lethality. Nevertheless, adverse risks such as inflammatory disease and tumor metastasis might be induced during the process.[7,8] In an attempt to down-regulate and suppress the expression of HSPs, different strategies have been developed, including the use of inhibitors and siRNAs.[9,10] Although the reported methods exhibited promising antitumor efficacy, the poor stability of siRNA, the potential toxicity and the hysteretic effect of inhibitors should not be ignored.[11] Therefore, it is necessary to find new methods that could effectively block the generation or inhibit the activity of HSPs.

Due to the intrinsic consumption of energetic adenosine triphosphate (ATP) during the HSP expression process, the hyperthermia resistance of tumor cells caused by HSPs might be overcome by constantly consuming ATP in a different way, further improving the efficacy of PTT. In contrast to normal tissue cells, a significant increase in glucose uptake is found in cancerous cells.[12] Tumor cells preferentially drive their own proliferation *via* anaerobic glycolysis, leading to less ATP generation and higher glucose internalization to meet the needs of nutrients and energy substances.[13–15] As a result, the proliferation and progression of malignant cancers are highly dependent on the supply of glucose. In recent years, cancer

[a] *Tianjin Key Laboratory of Drug Targeting and Bioimaging, Life and Health Intelligent Research Institute, Tianjin University of Technology, Tianjin 300384, China. E-mail: wei_zhang@email.tjut.edu.cn*
[b] *Biomedical Polymers Laboratory, College of Chemistry, Chemical Engineering and Materials Science, and State Key Laboratory of Radiation Medicine and Protection, Soochow University, Suzhou 215123, China*
[c] *Key Laboratory of Chemo/Biosensing and Detection, College of Chemical and Materials Engineering, Xuchang University, Henan 461000, China*
[d] *State Key Laboratory of Polymer Physics and Chemistry, Changchun Institute of Applied Chemistry, Chinese Academy of Sciences, 5625 Renmin Street, Changchun, Jilin 130022, China. E-mail: suntt@ciac.ac.cn, xiez@ciac.ac.cn*

† Electronic supplementary information (ESI) available: Materials, instruments, experimental details, and spectral data. See DOI: https://doi.org/10.1039/d3qm00132f

starvation therapy (CST) has become an emerging treatment for malignant tumors by cutting off the blood supply of tumor tissues to inhibit the rapid growth of cancers.[16] Glucose oxidase (GOx) can efficiently catalyze the oxidation of glucose into glucose acid and hydrogen peroxide (H_2O_2),[17,18] which would significantly reduce ATP generation and might provide an adjuvant method for CST. The produced H_2O_2 could further transform into $^{\bullet}OH$ with stronger cytotoxicity by combining with the Fenton reaction,[19,20] promoting oxidative stress-induced apoptosis.[21,22] Although GOx has shown potential therapeutic effects in the treatment of tumor, its poor stability, strong systemic toxicity and rapid metabolism severely limit its direct applications *in vivo*. Therefore, how to effectively deliver exogenous GOx to cancer cells is of vital importance for achieving synergistic anticancer effects of starvation therapy and oxidation therapy.

To overcome the above challenges, we designed and fabricated imidazolyl-modified and positively charged conjugated polymers (IBDDP) as the PTAs, which could assemble into composite nanoparticles (IBDDP&GOx NPs) with GOx *via* electrostatic interactions, as illustrated in Scheme 1. Multiple experiments demonstrate that the prepared IBDDP&GOx NPs could not only maintain the primary catalytic activity of GOx but also exhibit satisfactory photothermal conversion ability. GOx displays synergistic effects in starvation therapy and oxidative therapy by continuously consuming glucose in cells and simultaneously producing a large amount of H_2O_2. As a cascade reaction, the production of ATP in tumor cells is severely interfered due to the consecutive consumption of glucose, further impeding the expression of HSPs and enhancing the PTT sensitivity to realize an ideal combined anticancer effect.

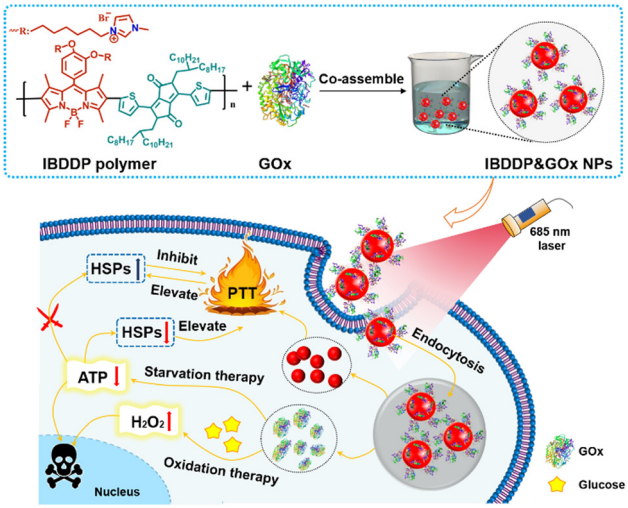

Scheme 1 Schematic illustration of the structure of the imidazolyl-substituted ionized BODIPY-based conjugated polymer (IBDDP), the nanosystem driven by the electrostatic interaction between the IBDDP and GOx, and its application in multimodal carcinoma therapy.

Results and discussion

The imidazolyl-substituted ionized IBDDP polymer was synthesized using the synthetic route shown in Fig. S1 (ESI†). Briefly, imidazolyl-substituted BODIPY was first prepared *via* a typical experimental procedure reported by our group.[23–25] Then, Suzuki coupling polymerization was carried out between diketopyrrolopyrrole derivative M1 and IBDP. After repeated precipitation in ice-cold methanol, a dark black imidazolyl-substituted and positively charged conjugated polymer, IBDDP, was obtained. The proton nuclear magnetic resonance (^{1}H NMR) spectra are shown in Fig. S2 and S3 (ESI†), demonstrating the successful synthesis of IBDDP. Considering the imidazole groups in the IBDDP backbone, the polymer chains are positively charged, enabling the formation of nanocomplexes with negatively charged GOx through electrostatic interactions. First, by means of the ultrasonic emulsification method, we prepared stable nanocomposites (IBDDP&GOx NPs) and then determined the optimal mixing ratio of IBDDP and GOx with different feeding ratios: IBDDP/GOx = 1/0, 1/3, 1/5, 2/1, 5/1, 10/1. As shown in Fig. S4A (ESI†), homogeneous and stable dispersions could be obtained by combining GOx with IBDDP, and less precipitation was formed along with an increase in GOx. Subsequently, the hydrated diameter, polydispersity index (PDI) and zeta potential of the abovementioned IBDDP&GOx NPs were characterized by dynamic light scattering (DLS). As shown in Fig. 1A, B and Fig. S4B (ESI†), the diameter and surface potential of IBDDP NPs formed by merely encapsulating IBDDP with the amphiphilic polymer F-127 were 138.3 nm and +37.4 mV, respectively, confirming the strong positive charge of the IBDDP polymer and the capability to interact with the negatively charged GOx. Moreover, as the concentration of GOx increased, the NPs became small, and the charge of the NPs changed from positive to negative. Some reported studies showed that NPs with a positive charge were more easily endocytosed than negatively charged NPs.[26–28] With regard to the efficient catalytic ability of GOx reported by other studies,[29,30] we decided to utilize the IBDDP&GOx NPs with a feeding ratio of 10 : 1 for all the experiments, and the surface charge was +30 mV. As shown in Fig. 1C,

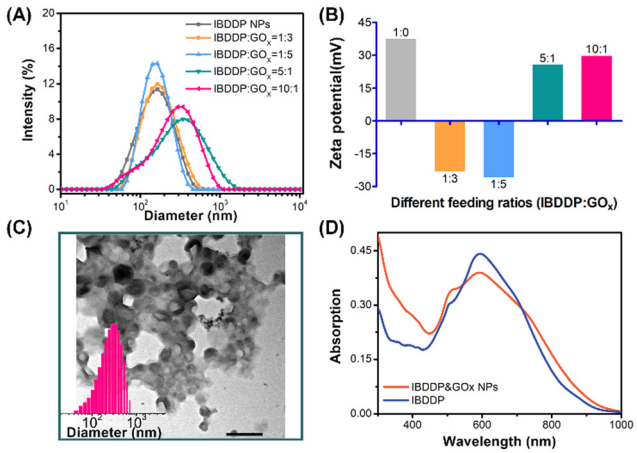

Fig. 1 (A) Size distribution and (B) surface potential of different nanocomplexes determined by DLS. (C) TEM image of the IBDDP&GOx NPs. Inset image: the size distribution of NPs measured by DLS; scale bar: 500 nm. (D) UV-vis-NIR absorption spectra of the IBDDP&GOx NPs in aqueous solution and IBDDP in THF.

the transmission electron microscopy (TEM) image indicated that IBDDP&GOx NPs could assemble into spherical and uniform NPs with a diameter of 214.9 nm (inset picture in Fig. 1C) in aqueous solution. The size determined by TEM was slightly smaller than the hydrated diameter measured by DLS, which might be because that the TEM images were taken under a dry formulation. According to the UV-vis spectra and BCA (bicinchronic acid) protein quantitative assay kit, the concentrations of IBDDP and GOx were 710.3 μg mL^{-1} and 30.0 μg mL^{-1}, respectively (Fig. S5, ESI†). Furthermore, the changes in the diameters and PDIs were measured by DLS. The diameter and PDI of the IBDDP&GOx NPs remained unchanged over a week, which demonstrated that the IBDDP&GOx NPs exhibited good colloidal stability (Fig. S6A, ESI†). Furthermore, we also investigated the stability of IBDDP&GOx in PBS with 10% FBS at 37 °C. The size and PDI of the NPs remained consistent within 12 h, indicating the improved stability of IBDDP NPs after interacting with GOx (Fig. S6B, ESI†). As shown in Fig. 1D, the UV-vis-NIR absorption spectra of IBDDP and IBDDP&GOx NPs were characterized. The maximum absorption peak of IBDDP&GOx NPs was mainly located at 595 nm. Because of the formation of aggregates by IBDDP and GOx, the absorption spectrum of IBDDP&GOx NPs was broadened with a decreased absorbance compared with that of IBDDP. The fluorescence spectra of IBDDP&GOx NPs, IBDDP polymers and IBDP were also detected (Fig. S7, ESI†). The maximum fluorescence wavelength of IBDDP polymers (in THF) was observed at 821 nm, while much weaker fluorescence was observed for IBDDP&GOx NPs due to the phenomenon of aggregation-caused quenching (ACQ).[31]

To detect the enzymatic activity of GOx in the nanocomposites, the cascade reaction of horseradish peroxidase (HRP) and *o*-dianisidine was carried out (Fig. 2A).[32] As shown in Fig. 2B, the changes in the absorption intensity at 460 nm of newly produced reduced *o*-dianisidine were measured using a UV-vis spectrometer to obtain the kinetic curve of the whole reaction process, and the initial slope of the curve was used to evaluate the catalytic activity of GOx. An obvious characteristic absorption peak at 460 nm of oxidized *o*-dianisidine could be observed with the addition of GOx (1 μg mL^{-1}) and IBDDP&GOx NPs. As expected, the reaction efficiency of IBDDP&GOx NPs was slightly lower than that of GOx, which might be attributed to some destruction of GOx in the presence of THF during the NP preparation process. According to Fig. 2C, calculating the initial slope of the catalytic reaction curve as the catalytic capability of the GOx enzymatic reaction and defining that of pure GOx as 100%, the activity of IBDDP&GOx NPs can still be maintained at 61% and exhibit a concentration-dependent catalytic effect. Moreover, we could also directly observe the GOx-catalyzed cascade reaction through the solution color due to the production of brownish-yellow oxidized *o*-dianisidine (Fig. S8A, ESI†). Because of the large production of toxic H_2O_2 *via* the GOx-triggered decomposition of glucose, it could effectively oxidize and destroy biological macromolecules, such as proteins and DNA, simultaneously accompanied by the continuous consumption of the energetic glucose, and induce a starvation effect on the intracellular energy metabolism cycle and

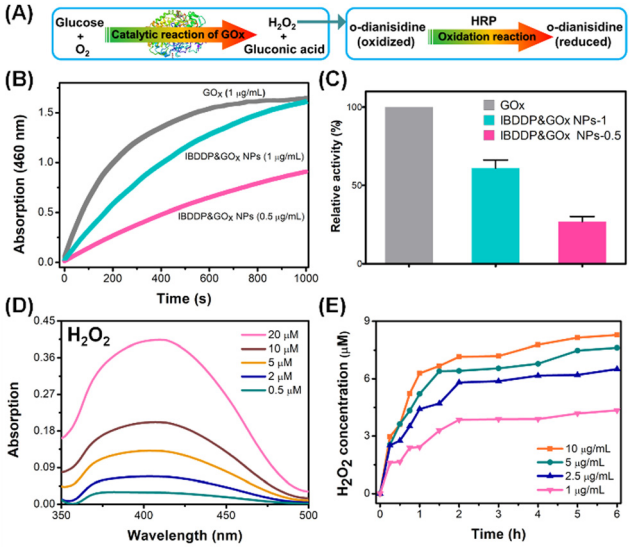

Fig. 2 (A) The reaction mechanism of GOx activity assays. (B) Time-dependent absorption spectra (Abs, 460 nm) of *o*-dianisidine after the cascade reactions. (C) Relative activities of GOx (1 μg mL^{-1}) and IBDDP&GOx NPs (GOx: 1 and 0.5 μg mL^{-1}), n = 3. (D) UV-vis absorption spectra of formed Ti(IV)OSO_4 at different H_2O_2 concentrations (0.5–20 μM). (E) H_2O_2 generated from the catalyzed reaction of glucose (100 μg mL^{-1}) in the presence of various IBDDP&GOx NPs (GOx: 1–10 μg mL^{-1}) at different time points.

eventually cellular apoptosis and necrosis.[33,34] Hence, we further evaluated the catalytic ability of IBDDP&GOx NPs to produce H_2O_2 from glucose at 37 °C. The concentration of the generated H_2O_2 was measured based on the formation of a yellow titanium peroxide complex ($Ti(IV)O_2^{2+}$) arising from the reaction of the colorless $Ti(IV)O^{2+}$ and H_2O_2, with a characteristic UV absorption peak at 407 nm.[35] As depicted in Fig. 2D and E, we measured H_2O_2 generation plots at a series of concentrations of IBDDP&GOx NPs according to the standard linear curve between H_2O_2 and the peak strength at 470 nm (Fig. S8B and C, ESI†). The production of H_2O_2 was accelerated along with the increase in NPs and basically reached equilibrium after 3 h. Based on the above data, we concluded that IBDDP&GOx NPs can effectively decompose glucose, providing theoretical potential for further eliminating cancer cells *via* CST and H_2O_2-induced oxidative therapy.

Furthermore, we evaluated the photothermal properties of IBDDP&GOx NPs by examining the temperature changes at various IBDDP concentrations and laser fluences. As expected, exposing the NP solution (IBDDP: 50 μg mL^{-1}) to the 685 nm laser (0.61 W cm^{-2}) for 5 min, the temperature was elevated by 35 °C. As a comparison, pure water showed an inconspicuous temperature change under the same circumstances. In addition, the photothermal properties of IBDDP&GOx NPs were concentration- and laser power-dependent (Fig. 3A, B and D). Moreover, five continual laser irradiation/cooling cycles were carried out on the NP solutions, indicating excellent photothermal stability without obvious deterioration (Fig. 3C). The photothermal conversion efficiency (η) of IBDDP&GOx NPs was calculated to be 23.1% (Fig. S9A and C, ESI†).[36] In addition, we

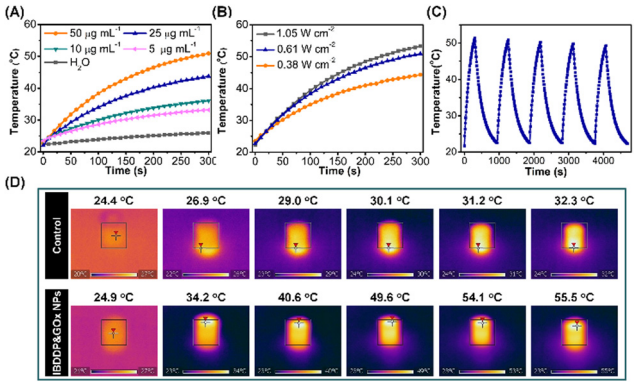

Fig. 3 Heating-up curves of IBDDP&GOx NPs at (A) different concentrations (5–50 μg mL^{-1}) and (B) laser power densities (0.38–1.05 W cm^{-2}) as a function of irradiation time. (C) Heating reproducibility of IBDDP&GOx NP solution (50 μg mL^{-1}) over multiple laser on/off cycles under a 685 nm (0.61 W cm^{-2}) laser irradiation. (D) Thermal images of IBDDP&GOx NPs (IBDDP: 50 μg mL^{-1}) and aqueous solution under a 685 nm laser irradiation of 0.61 W cm^{-2} at different time points, respectively.

also measured the photothermal performance of IBDDP NPs, and the results showed that IBDDP&GOx NPs and IBDDP NPs had similar photothermal activities, implying that the photothermal properties of IBDDP were not affected after forming NPs with GOx (Fig. S9B, D and S10, ESI†). All these results confirmed that IBDDP&GOx NPs possess an outstanding NIR photothermal effect with excellent photostability and could be potential candidates for photothermal therapy.

Efficient endocytosis of NPs by tumor cells is generally a prerequisite for cellular toxicity. Thus, we first utilized confocal laser scanning microscopy (CLSM) and flow cytometry (FCM) to study the intercellular uptake of IBDDP&GOx NPs. As shown in Fig. 4A and Fig. S11A (ESI†), cervical cancer HeLa cells exhibited obvious red fluorescence, and the endocytosis of IBDDP&GOx NPs increased as time went and the temperature increased from 4 to 37 °C. To explain the specific endocytic pathway of the NPs in detail, HeLa cells were pretreated with a series of inhibitors: amiloride (micropinocytosis), glucose (clathrin-mediated), genistein (caveolin-mediated) and Na_3N (energy-dependent) and analyzed by FCM for the endocytosis ability

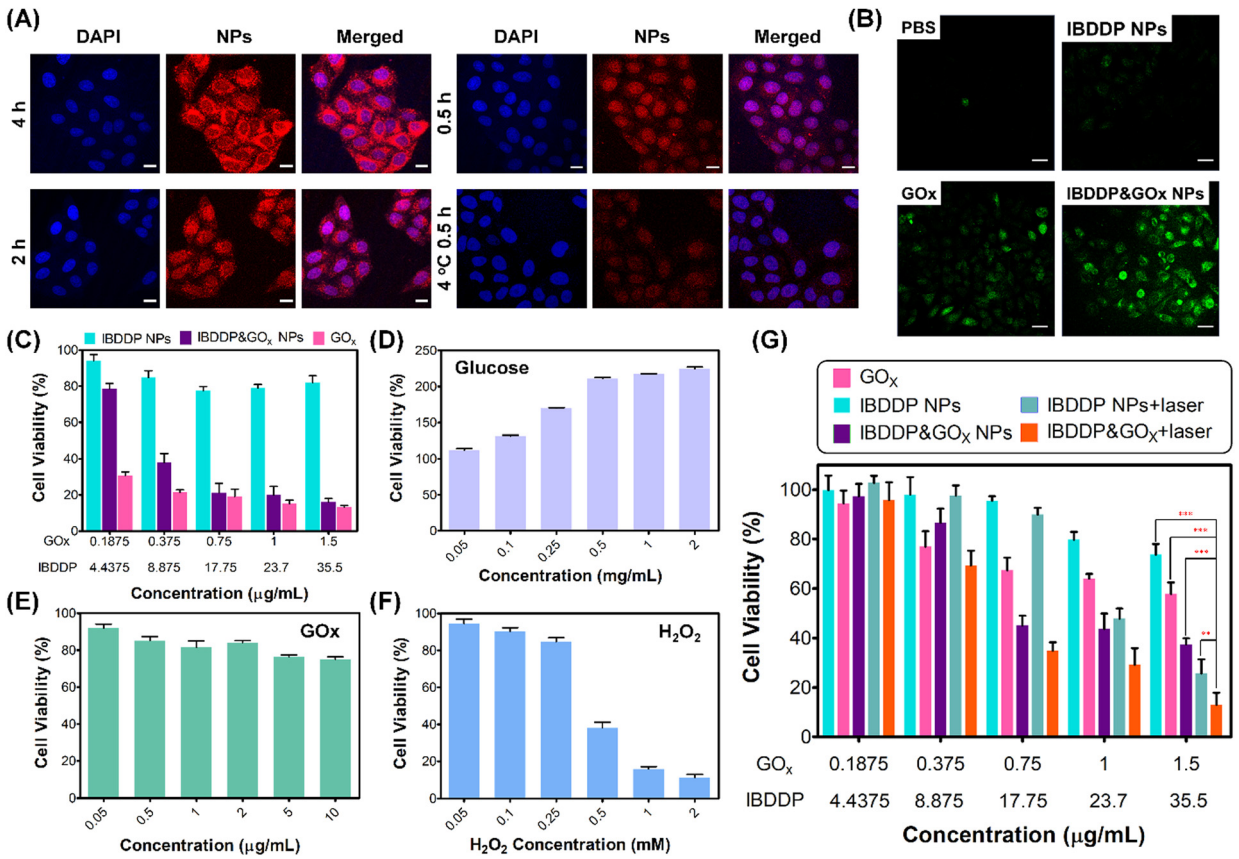

Fig. 4 (A) CLSM results of HeLa cells incubated with IBDDP&GOx NPs (IBDDP: 20 μg mL^{-1}) at 37 °C for 0.5, 2 and 4 h and at 4 °C for 0.5 h; scale bar: 20 μm. (B) ROS production of HeLa cells after treatment with IBDDP NPs (23.7 μg mL^{-1}), GOx (1 μg mL^{-1}) and IBDDP&GOx NPs (IBDDP: 23.7 μg mL^{-1} and GOx: 1 μg mL^{-1}); scale bar: 40 μm. (C) Cytotoxicities of IBDDP NPs, GOx and IBDDP&GOx NPs toward HeLa cells without laser irradiation in a normal medium, n = 4. Cell viabilities of HeLa cells after treatment with different concentrations of (D) glucose and (E) GOx in the glucose-free DMEM, n = 4. (F) Cell viabilities of HeLa cells after treatment with H_2O_2 in a normal medium, n = 4. (G) Cell viabilities of HeLa cells treated with different concentrations of IBDDP NPs, GOx or IBDDP&GOx NPs in the low-glucose DMEM in the presence of laser irradiation (685 nm, 0.61 W cm^{-2}, 7 min), n = 4. All the data are shown as the average value ± SD. Unless stated otherwise, experiments were implemented in triplicate. The significance of the difference was decided through one-way analysis of variance (*$p < 0.05$, **$p < 0.01$, and ***$p < 0.001$).

of the NPs.[37–39] The fluorescence intensity of IBDDP&GOx NPs significantly decreased after glucose, genistein and Na_3N treatment, indicating that the nanoparticles were mainly endocytosed into tumor cells in an energy-dependent clathrin- and caveolin-mediated manner (Fig. S11B, ESI†). Furthermore, we examined the intracellular H_2O_2 generation ability of IBDDP&GOx NPs by the ROS detection probe 2′,7′-dichlorofluorescein diacetate (DCFH-DA). According to Fig. 4B, stronger green fluorescence could be observed in HeLa cells treated with IBDDP&GOx NPs than in those treated with GOx and PBS. More importantly, the fluorescence intensity of IBDDP&GOx NPs was significantly higher than that of IBDDP NPs. Therefore, we were able to confirm that the nanocomposite IBDDP&GOx NPs could indeed generate H_2O_2 by depleting glucose.

Inspired by the favorable results above, we further investigated the synergistic therapeutic effects of HeLa cells by monitoring the viability after incubation with IBDDP&GOx NPs *via* 3-(4,5-dimethylthiazol-2-yl)-2,5-diphenyltetrazolium bromide (MTT) assays. We first investigated the cytotoxicity of IBDDP&GOx NPs, IBDDP NPs and GOx in the absence of laser irradiation at different concentrations in the normal Dulbecco's modification of Eagle's medium (DMEM). As shown in Fig. 4C, IBDDP NPs exhibited good biocompatibility without temperature variations. However, due to the existence of GOx and high glucose (4.5 mg mL^{-1}) in the DMEM, the IBDDP&GOx NP and GOx groups could produce a large amount of H_2O_2 and induce massive cellular death. Even with an extremely low GOx concentration (0.375 μg mL^{-1}), the viability of HeLa cells in both the IBDDP&GOx NP and GOx groups decreased below 40%. To further validate that the strong cytotoxicity of IBDDP&GOx NPs was definitely caused by the synergistic effect of CST and oxidative therapy, we also separately determined the biocompatibility of glucose, GOx and H_2O_2 under different treatments. As shown in Fig. 4D, after incubation in the glucose-free DMEM, the addition of glucose could indeed promote the proliferation of tumor cells, while with doping of 10 μg mL^{-1} GOx, 20% cellular death could still be observed (Fig. 4E). We speculated that the slight toxicity of GOx in the glucose-free DMEM was mainly caused by the continuous consumption of glucose *via* the disruption of the glucose metabolism, thereby inhibiting the proliferation of HeLa cells. In addition, we also investigated the effect of H_2O_2 on cancer cells in the normal DMEM. Fig. 4F shows that more cellular death could be induced with the increase of H_2O_2 to increase oxidative stress. To further optimize the MTT results and considering the high cytotoxicity of IBDDP&GOx NPs in the traditional DMEM and the unsatisfactory toxicity of GOx in the glucose-free cellular medium, we evaluated the trimodal anticancer effect (CST, PTT and oxidative therapy) of IBDDP&GOx NPs in the low-glucose DMEM (1 mg mL^{-1}). As characterized in Fig. 4G, in the absence of laser irradiation, the cell viability exhibited a negligible decrease after incubation with IBDDP NPs, whereas an apparent decrease could be observed for IBDDP&GOx NPs due to the consumption of glucose and production of oxidative substances. Moreover, IBDDP NPs exhibited good photothermal toxicity under light irradiation, and the cell viability was only 25% with 35.5 μg mL^{-1} IBDDP. However, under the same conditions, the IBDDP&GOx NPs presented enhanced cellular toxicity compared with the IBDDP NP group for only photothermal therapy and the GOx group for starvation therapy. To further intuitively characterize the synergistic antitumor effects of IBDDP&GOx NPs, live/dead cell staining and trypan blue staining were carried out (Fig. S12 and S13, ESI†). As shown in Fig. S12 (ESI†), most of the cells in all groups showed green fluorescence without laser irradiation. However, it is noteworthy that the morphology of tumor cells in the IBDDP&GOx NP group was significantly different from that in the other groups, mainly due to the presence of GOx. Under laser irradiation, IBDDP&GOx NPs displayed more obvious red fluorescence than IBDPP NPs, indicating the highest cellular death. Fig. S13 (ESI†) shows results similar to those of live/dead cell staining. With the treatment of IBDDP&GOx NPs, obvious cellular membrane shrinkage could be observed. Based on these preliminary results, we concluded that IBDDP&GOx NPs exhibited the most satisfactory antitumor performance and showed distinct cellular shrinkage compared with the other groups, which proved that IBDDP&GOx NPs could indeed achieve a synergistic strategy *via* the combination of PTT, CST and oxidative therapy. Furthermore, the JC-1 probe was utilized to determine the damage of the mitochondrial membrane of HeLa cells caused by IBDDP&GOx NPs. In general, when the mitochondria are complete, the mitochondrial membrane potential is high, showing red fluorescence due to the aggregation formation of JC-1, while typical green fluorescence could be observed when mitochondria are damaged with the decrease of the mitochondrial membrane potential. As shown in Fig. S14 (ESI†), IBDDP NPs can damage the mitochondria *via* laser irradiation. However, the mitochondria of the cells treated with IBDDP&GOx NPs can be damaged either with or without laser irradiation.

It is well known that glucose is the main energy substance of animals and plants, and aerobic respiration is the most important biological metabolism of glucose, simultaneously releasing energy and synthesizing a large amount of ATP.[40] As a result, the glucose content in cells directly affects the expression of ATP. Therefore, we further evaluated the expression of intracellular ATP in HeLa cell posttreatment with IBDDP&GOx NPs and IBDDP NPs. A luminometer was used to measure the chemiluminescence intensity of ATP as the standard, and the result is shown in Fig. S15 (ESI†). The chemiluminescence intensity increased linearly with more ATP. Subsequently, HeLa cells were coincubated with IBDDP&GOx NPs and IBDDP NPs. As characterized in Fig. 5A, after treatment with IBDDP&GOx NPs, the intracellular ATP of HeLa cells was significantly decreased but had little effect on the IBDDP NP group, which indicated that the functionalized IBDDP&GOx NPs could reduce glucose uptake *via* GOx-mediated CST, causing ATP production disorder and interrupting the energy metabolism in cancer cells. As a cascade reaction, the content of ATP in cells further affects protein expression. In this work, we focused on the expression of HSPs, a group of proteins with self-protection mechanisms produced by malignant cells under external

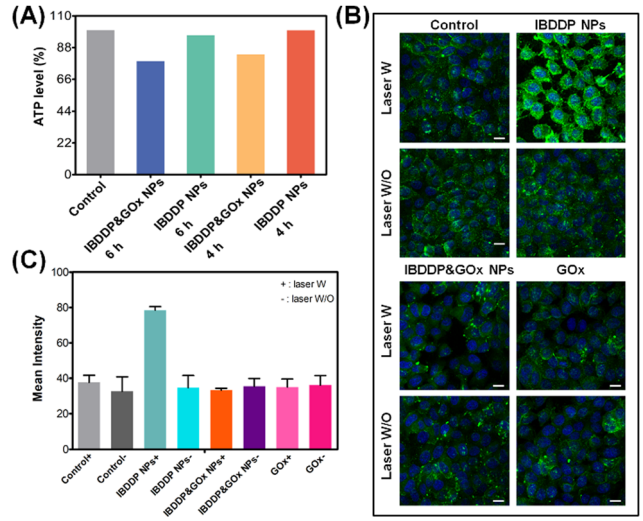

Fig. 5 (A) ATP expression of HeLa cells after treatment with IBDDP&GOx NPs (IBDPDP: 35.5 μg mL^{-1} and GOx: 1.5 μg mL^{-1}) and IBDDP NPs for 4 and 6 h, respectively. (B) Expression of HSP90 in HeLa cells with different treatments after incubation for 1 h determined by immunofluorescence staining. The cells were treated with PBS, IBDDP&GOx NPs, IBDDP NPs and GOx under a 658 nm laser irradiation (0.61 W cm^{-2}, 7 min); scale bar: 20 μm. (C) Mean intensity of immunofluorescence images for HSP90, n = 3.

stimuli, which are closely related to the tumor cell killing performance of PTT. Therefore, the immunofluorescence analysis of HSP90, a representative protein of the HSP family, was selected to evaluate the impact of different nanocomposites on the expression of HSPs. Fig. 5B and C show that the expression of HSP90 was significantly upregulated (stronger green fluorescence) owing to the increased temperature during the PTT process. However, after treatment with IBDDP&GOx NPs and GOx, the expression level of HSP90 in HeLa cells was much lower than that of IBDDP NPs under laser irradiation. To further quantitatively confirm the HSP90 inhibition effect of IBDDP&GOx NPs, the western blotting assay was carried out to examine the level of HSP90 in HeLa cells. As demonstrated in Fig. S16 (ESI†), the expression of HSP90 was significantly upregulated for IBDDP NPs under laser irradiation, while for the cells treated with GOx and IBDDP&GOx NPs, the expression of HSP90 was down-regulated obviously, indicating the effect of GOx induced CST with glucose and ATP decrease inhibiting HSP90 expression, which was consistent with the results shown in Fig. 5B and C. The above results strongly support that GOx could effectively suppress the HSP expression, which provided a potential pathway to boost PTT.

Conclusions

In this study, multimodal anti-carcinoma nanocomplexes, IBDDP&GOx NPs, were prepared using glucose oxidase and BODIPY-based conjugated polymers for combined starvation therapy, oxidation therapy and photothermal therapy. Compared with single photothermal treatment or starvation therapy, IBDDP&GOx NPs demonstrated much higher antitumor capability. The IBDDP-conjugated polymer could effectively convert laser energy into local high temperature and then induce excessive cancer apoptosis. On the other hand, the introduction of GOx could not only produce H_2O_2 by constantly consuming glucose but also decrease the expression of energetic ATP and ATP-dependent HSPs in tumor cells, which further assists photothermal therapy. This work provides a new design idea for improving the PTT effect of conjugated polymers and combining more diversified therapeutic methods.

Author contributions

Dr W. Zhang designed the experiments, synthesized the targeted product, participated in all the experiments, analyzed the data and wrote the draft of the manuscript; Dr W. Lin provided assistance to the entire Experimental section and contributed to the discussion; Prof. Z. Li was mainly responsible for paper reviewing and funding acquisition; Prof. T. Sun and Prof. Z. Xie conceived the idea and supervised and funded the research project. All the authors contributed to the data analysis and discussion of the manuscript.

Conflicts of interest

The authors declare no competing financial interest.

Acknowledgements

This project was supported by the National Natural Science Foundation of China (Project No. 51522307 and No. 22205161) and the Key Scientific Research Projects of Universities in Henan Province (No: 21A150052).

Notes and references

1 S. Wang, Y. Tian, W. Tian, J. Sun, S. Zhao, Y. Liu, C. Wang, Y. Tang, X. Ma and Z. Teng, Selectively sensitizing malignant cells to photothermal therapy using a CD44-targeting heat shock protein 72 depletion nanosystem, *ACS Nano*, 2016, **10**, 8578–8590.
2 X. Deng, K. Li, X. Cai, B. Liu, Y. Wei, K. Deng, Z. Xie, Z. Wu, P. A. Ma and Z. Hou, A hollow-structured CuS@Cu$_2$S@Au nanohybrid: synergistically enhanced photothermal efficiency and photoswitchable targeting effect for cancer theranostics, *Adv. Mater.*, 2017, **29**, 1701266.
3 S. Zhang, W. Guo, J. Wei, C. Li, X.-J. Liang and M. Yin, Terrylenediimide-based intrinsic theranostic nanomedicines with high photothermal conversion efficiency for photoacoustic imaging-guided cancer therapy, *ACS Nano*, 2017, **11**, 3797–3805.
4 B.-K. Wang, X.-F. Yu, J.-H. Wang, Z.-B. Li, P.-H. Li, H. Wang, L. Song, P. K. Chu and C. Li, Gold-nanorods-siRNA nanoplex for improved photothermal therapy by gene silencing, *Biomaterials*, 2016, **78**, 27–39.
5 G. Gao, Y. W. Jiang, Y. Guo, H. R. Jia, X. Cheng, Y. Deng, X. W. Yu, Y. X. Zhu, H. Y. Guo and W. Sun, Enzyme-

mediated tumor starvation and phototherapy enhance mild-temperature photothermal therapy, *Adv. Funct. Mater.*, 2020, **30**, 1909391.

6 H. Zhu, X. Cao, X. Cai, Y. Tian, D. Wang, J. Qi, Z. Teng, G. Lu, Q. Ni and S. Wang, Pifithrin-μ incorporated in gold nanoparticle amplifies pro-apoptotic unfolded protein response cascades to potentiate synergistic glioblastoma therapy, *Biomaterials*, 2020, **232**, 119677.

7 X. Zhu, W. Feng, J. Chang, Y.-W. Tan, J. Li, M. Chen, Y. Sun and F. Li, Temperature-feedback upconversion nanocomposite for accurate photothermal therapy at facile temperature, *Nat. Commun.*, 2016, **7**, 1–10.

8 Y. Yang, W. Zhu, Z. Dong, Y. Chao, L. Xu, M. Chen and Z. Liu, 1D coordination polymer nanofibers for low-temperature photothermal therapy, *Adv. Mater.*, 2017, **29**, 1703588.

9 F. Ding, X. Gao, X. Huang, H. Ge, M. Xie, J. Qian, J. Song, Y. Li, X. Zhu and C. Zhang, Polydopamine-coated nucleic acid nanogel for siRNA-mediated low-temperature photothermal therapy, *Biomaterials*, 2020, **245**, 119976.

10 H. Luo, Q. Wang, Y. Deng, T. Yang, H. Ke, H. Yang, H. He, Z. Guo, D. Yu and H. Wu, Mutually synergistic nanoparticles for effective thermo-molecularly targeted therapy, *Adv. Funct. Mater.*, 2017, **27**, 1702834.

11 W.-H. Chen, G.-F. Luo, Q. Lei, S. Hong, W.-X. Qiu, L.-H. Liu, S.-X. Cheng and X.-Z. Zhang, Overcoming the heat endurance of tumor cells by interfering with the anaerobic glycolysis metabolism for improved photothermal therapy, *ACS Nano*, 2017, **11**, 1419–1431.

12 D. Hanahan and R. A. Weinberg, Hallmarks of cancer: the next generation, *Cell*, 2011, **144**, 646–674.

13 R. Zhang, L. Feng, Z. Dong, L. Wang, C. Liang, J. Chen, Q. Ma, Q. Chen, Y. Wang and Z. Liu, Glucose & oxygen exhausting liposomes for combined cancer starvation and hypoxia-activated therapy, *Biomaterials*, 2018, **162**, 123–131.

14 Y. Ma, Y. Zhao, N. K. Bejjanki, X. Tang, W. Jiang, J. Dou, M. I. Khan, Q. Wang, J. Xia and H. Liu, Nanoclustered cascaded enzymes for targeted tumor starvation and deoxygenation-activated chemotherapy without systemic toxicity, *ACS Nano*, 2019, **13**, 8890–8902.

15 C. Bubici and S. Papa, The Warburg effect regulation under siege: the intertwined pathways in health and disease, *Front. Cell Dev. Biol.*, 2019, **7**, 80.

16 S. Guo and D. S. Kohane, Nanoparticulate cancer-starvation therapy, *Chemistry*, 2017, **2**, 168–170.

17 J.-J. Hu, M.-D. Liu, F. Gao, Y. Chen, S.-Y. Peng, Z.-H. Li, H. Cheng and X.-Z. Zhang, Photo-controlled liquid metal nanoparticle-enzyme for starvation/photothermal therapy of tumor by win-win cooperation, *Biomaterials*, 2019, **217**, 119303.

18 L. H. Fu, C. Qi, Y. R. Hu, J. Lin and P. Huang, Glucose oxidase-instructed multimodal synergistic cancer therapy, *Adv. Mater.*, 2019, **31**, 1808325.

19 L. Zhang, S.-S. Wan, C.-X. Li, L. Xu, H. Cheng and X.-Z. Zhang, An adenosine triphosphate-responsive autocatalytic Fenton nanoparticle for tumor ablation with self-supplied H_2O_2 and acceleration of Fe(III)/Fe(II) conversion, *Nano Lett.*, 2018, **18**, 7609–7618.

20 X. Meng, F. Zhang, H. Guo, C. Zhang, H. Hu, W. Wang, J. Liu, X. Shuai and Z. Cao, One-pot approach to Fe^{2+}/Fe^{3+}-based MOFs with enhanced catalytic activity for Fenton reaction, *Adv. Healthcare Mater.*, 2021, **10**, 2100780.

21 H. Yamakawa, Y. Ito, T. Naganawa, Y. Banno, S. Nakashima, S.-I. Yoshimura, M. Sawada, Y. Nishimura, Y. Nozawat and N. Sakai, Activation of caspase-9 and-3 during H_2O_2-induced apoptosis of PC12 cells independent of ceramide formation, *Neurol. Res.*, 2000, **22**, 556–564.

22 F. Yang, C. Song, R. Ji, X. Song, B. Yang, Y. Lv and Z. Wei, Increasing the production of reactive oxygen species through a ferroptosis pathway disrupts the redox balance of tumor cells for cancer treatment, *ACS Appl. Polym. Mater.*, 2022, **4**, 5001–5011.

23 W. Zhang, W. Lin, Q. Pei, X. Hu, Z. Xie and X. Jing, Redox-hypersensitive organic nanoparticles for selective treatment of cancer cells, *Chem. Mater.*, 2016, **28**, 4440–4446.

24 T. Sun, X. Guan, M. Zheng, X. Jing and Z. Xie, Mitochondria-localized fluorescent BODIPY-platinum conjugate, *ACS Med. Chem. Lett.*, 2015, **6**, 430–433.

25 W. Lin, W. Zhang, S. Liu, Z. Li, X. Hu, Z. Xie, C. Duan and G. Han, Engineering pH-responsive BODIPY nanoparticles for tumor selective multimodal imaging and phototherapy, *ACS Appl. Mater. Interfaces*, 2019, **11**, 43928–43935.

26 S. Jeon, J. Clavadetscher, D.-K. Lee, S. V. Chankeshwara, M. Bradley and W.-S. Cho, Surface charge-dependent cellular uptake of polystyrene nanoparticles, *Nanomaterials*, 2018, **8**, 1028.

27 Y. Liu, J. Zhang, Y. Tu and L. Zhu, Potential-independent intracellular drug delivery and mitochondrial targeting, *ACS Nano*, 2021, **16**, 1409–1420.

28 Y. Qiu, Y. Liu, L. Wang, L. Xu, R. Bai, Y. Ji, X. Wu, Y. Zhao, Y. Li and C. Chen, Surface chemistry and aspect ratio mediated cellular uptake of Au nanorods, *Biomaterials*, 2010, **31**, 7606–7619.

29 Y. Yang, Y. Lu, P. L. Abbaraju, I. Azimi, C. Lei, J. Tang, M. Jambhrunkar, J. Fu, M. Zhang and Y. Liu, Stepwise degradable nanocarriers enabled cascade delivery for synergistic cancer therapy, *Adv. Funct. Mater.*, 2018, **28**, 1800706.

30 J. Ming, T. Zhu, W. Yang, Y. Shi, D. Huang, J. Li, S. Xiang, J. Wang, X. Chen and N. Zheng, Pd@Pt-GOx/HA as a novel enzymatic cascade nanoreactor for high-efficiency starving-enhanced chemodynamic cancer therapy, *ACS Appl. Mater. Interfaces*, 2020, **12**, 51249–51262.

31 C. Wang, Z. Wang, S. Chen, P. Cui, L. Qiu, S. Zhou, H. Jiang, P. Jiang and J. Wang, Modulation of aggregation-caused quenching to aggregation-induced emission: finding a biocompatible polymeric theranostics platform for cancer therapy, *Macromol. Rapid Commun.*, 2021, **42**, 2100264.

32 D. Li, Q. He, Y. Cui, L. Duan and J. Li, Immobilization of glucose oxidase onto gold nanoparticles with enhanced thermostability, *Biochem. Biophys. Res. Commun.*, 2007, **355**, 488–493.

33 Z. Tang, Y. Liu, M. He and W. Bu, Chemodynamic therapy: tumour microenvironment-mediated Fenton and Fenton-like reactions, *Angew. Chem., Int. Ed.*, 2019, **58**, 946–956.

34 E. Hwang and H. S. Jung, Metal-organic complex-based chemodynamic therapy agents for cancer therapy, *Chem. Commun.*, 2020, **56**, 8332–8341.
35 W. Fan, N. Lu, P. Huang, Y. Liu, Z. Yang, S. Wang, G. Yu, Y. Liu, J. Hu and Q. He, Glucose-responsive sequential generation of hydrogen peroxide and nitric oxide for synergistic cancer starving-like/gas therapy, *Angew. Chem.*, 2017, **129**, 1249–1253.
36 Y. Liu, K. Ai, J. Liu, M. Deng, Y. He and L. Lu, Dopamine-melanin colloidal nanospheres: an efficient near-infrared photothermal therapeutic agent for in vivo cancer therapy, *Adv. Mater.*, 2013, **25**, 1353–1359.
37 M. Lira-Nogueira, V. Gibson, V. Nicolas, N. Santos-Magalhães and C. Vauthier, Defining endocytic pathways of Fucoidan-coated PIBCA nanoparticles from the design of their surface architecture, *Pharm. Res.*, 2022, **39**, 1–16.
38 R. B. Al-Humaidi, B. Fayed, S. B. Shakartalla, J. Jagal, M. N. Jayakumar, Z. M. Al Shareef, S. I. Sharif, A. Noreddin, M. H. Semreen and H. A. Omar, Optimum inhibition of MCF-7 breast cancer cells by efficient targeting of the macropinocytosis using optimized paclitaxel-loaded nanoparticles, *Life Sci.*, 2022, **305**, 120778.
39 H. Chen, Q. Guo, Y. Chu, C. Li, Y. Zhang, P. Liu, Z. Zhao, Y. Wang, Y. Luo and Z. Zhou, Smart hypoxia-responsive transformable and charge-reversible nanoparticles for the deep penetration and tumor microenvironment modulation of pancreatic cancer, *Biomaterials*, 2022, **287**, 121599.
40 G. Gottschalk, How escherichia coli synthesizes ATP during aerobic growth on glucose, *Bacterial Metabolism*, Springer, 1986, pp. 12–36.